Understanding the Weakening Relationship of the Pacific Decadal Oscillation and Indian Ocean Basin Mode During Boreal Winter

Jin-Sil Hong
Hanyang University - Ansan Campus
Sang-Wook Yeh (swyeh@hanyang.ac.kr)
Hanyang University https://orcid.org/0000-0003-4549-1686
Young-Min Yang
NUIST: Nanjing University of Information Science and Technology
Young-Kwon Lim
NASA
Kyu-Myong Kim
NASA

Research Article

Keywords: PDO, IOBM, Indo-Pacific relationship, Inter-basin Interactions, Decadal variability

Posted Date: June 25th, 2021

DOI: https://doi.org/10.21203/rs.3.rs-640927/v1

Abstract

While it is known that the Pacific Decadal Oscillation (PDO) leads the Indian Ocean Basin Mode (IOBM) with the same phase via the atmospheric bridge, we found that the relationship of PDO-IOBM during boreal winter is not stationary. Here, we investigated the PDO-IOBM relationship changes on low-frequency timescales by analyzing the observations, a long-term simulation of climate model with its large ensembles as well as the pacemaker experiments. A long-term simulation of climate model with its large ensemble simulations indicated that the non-stationary relationship of PDO-IOBM is intrinsic in a climate system and it could be at least partly due to internal climate variability. In details, we compared the PDO structures during the entire period with those during the period when the PDO-IOBM relationship was weak (i.e., 1976-2006). We found that the structures of sea surface temperature (SST) as well as its associated tropical Pacific convective forcing during the negative phase of PDO for 1976-2006 are far away from the typical structures of the negative PDO phase during the entire period, which were responsible for the weakening relationship of the PDO-IOBM in the observation. The results of the two pacemaker experiments support that a non-stationary relationship of PDO-IOBM is primarily due to the SST forcing in the Pacific.

1. Introduction

A number of climate variabilities on time scales from intra-seasonal to multi-decadal exist in the Indo-Pacific regions (Chowdary et al. 2012; Krishnamurthy and Goswami 2000; Sui et al. 2007; Waliser et al. 2003), and they affect the weather and climate in the globe as well as that of their surrounding region via oceanic and atmospheric teleconnections (Ummenhofer et al. 2013). Among them, the low-frequency variability of sea surface temperature (SST) in the Pacific and Indian Ocean basins also exists, i.e., Pacific Decadal Oscillation (PDO)/Interdecadal Pacific Oscillation (IPO), and Indian Ocean Basin Mode (IOBM).

PDO, which is primarily due to ocean-atmosphere interactions in the North Pacific, is the most dominant SST variability on a decadal time scale in the Pacific Ocean (Mantua and Hare 2002; Newman et al. 2016; Schneider and Cornuelle 2005). On the other hand, IOBM features basin-wide warming or cooling in the Indian Ocean (Guo et al. 2018; Han et al. 2014b). PDO affects the climate of the Northern Hemisphere, including East Asian monsoons and the Indian summer monsoons, and the North Pacific ecosystem on a decadal time scale (Chan and Zhou 2005; Chen et al. 2013; Hare and Mantua 2001; Hessl et al. 2004; Krishnamurthy and Krishnamurthy 2014; Krishnan and Sugi 2003; Wang et al. 2008), Previous literature has also shown that IOBM also influences East Asian monsoon variability by modulating the East Asian jet and the intensity of the South Asian high (Chowdary et al. 2011; Huang et al. 2011; Qu and Huang 2012; Xie et al. 2009; Yang et al. 2007). Therefore, it is essential to understand the relationship of PDO-IOBM to clarify their influences on the regional weather and climate variability.

In general, Pacific decadal variability including the PDO/IPO affects the Indian Ocean via atmospheric and oceanic teleconnections (Cole et al. 2000; Crueger et al. 2009, Huang et al., 2019, Lee et al., 2015).

Statistically, the PDO/IPO is positively correlated with the IOBM, i.e., a positive phase of PDO/IPO is concurrent with a basin-wide warming of the Indian Ocean, and vice versa (Klein et al. 1999). However, recent studies suggest the changes in the relationship of PDO/IOBM and IOBM. For example, Dong; McPhaden (2017) argued that the relationship between IPO and IOBM has been weakened by external anthropogenic forcing. By analyzing Coupled Model Intercomparison Phase 5 climate models, they suggested that the external forcing strongly influenced the Indian Ocean basin warming more than IPO, resulting in a strengthening of the out-of-phase relationship of IPO-IOBM. This result indicated that the relationship of IPO and IOBM could be modulated by anthropogenic forcing. Han et al. (2014a) suggested that a strengthening of the out-of-phase relationship between the IPO and IOBM since 1985 led to an intensified sea-level variability in the western tropical Pacific. Cai et al. (2019) and Wang (2019) also suggested that understanding the ocean basin interactions including the Pacific, Indian, and Atlantic is important for improving climate prediction and future climate projections. These require a further understanding of the changes in the relationship of PDO/IPO and IOBM. In this study, we investigated the relationship of PDO and IOBM, and we found that their relationship is not stationary on low-frequency timescales. The main purpose of this study is to investigate the mechanisms associated with the weakening relationship of PDO and IOBM in the observation, which received less attention compared to the relationship of IPO and IOBM as mentioned above.

This paper is organized as follows. Section 2 describes the data, definitions, and model design used in the analysis. Section 3 examines the causes of the weakening of the PDO-IOBM relationships from observation, reanalysis, and model results. Section 4 includes the summary and discussion.

2. Data And Methodology

a. Dataset

We used monthly SST from the Hadley Centre Global Sea Ice and SST version 1.1 (HadISST1.1), gridded at a 1° latitude x 1° longitude resolution (Rayner et al. 2003) and the Extended Reconstructed Sea Surface Temperature version 4 (ERSSTv4), gridded at a 2° latitude x 2° longitude resolution (Huang et al. 2015; Liu et al. 2015). The atmospheric datasets including air temperature, omega, and wind are obtained from the National Center for Environmental Prediction and National Center for Atmospheric Research (NCEP/NCAR) Reanalysis-1 dataset, gridded at a 2.5° latitude x 2.5° longitude resolution (Kalnay et al. 1996). For the precipitation dataset, NOAA's Precipitation Reconstruction (PREC) at a 1° latitude x 1° longitude was used (Chen et al. 2004). We primarily focused on the boreal winter season (December, January, February, hereafter, DJF), when both the PDO and the IOBM are dominant (Alexander et al. 2002; Huang et al. 2019; Schott et al. 2009). All of the datasets covered the period of 1948 to 2018 and the DJF mean was calculated from the monthly data from December to February. The seasonal anomaly was obtained by subtracting the winter-mean from the total winter-mean field and the linear trend was removed.

b. Definition of PDO, IOBM, and their indices

The PDO is defined by the first empirical orthogonal function (EOF) mode of sea surface temperature (SST) anomalies in the North Pacific basin (poleward of 20°N) (Mantua and Hare 2002) and the PDO index is defined as its corresponding principal component (PC) time series. On the other hand, the IOBM index is defined as the SST anomalies averaged in the Indian Ocean basin (45°S-20°N, 30°E-120°E) (Han et al. 2014b; Zhang et al. 2018a). It should be noted that the PDO index and the IOBM index are standardized by their standard deviations.

c. Pacemaker experiment using the NESMv3

We conducted a pacemaker experiment using the Nanjing University of Information Science and Technology Earth System Model version 3 (NESMv3) model (Cao et al. 2018) with four ensemble members. The NESM v3 consists of the atmospheric model ECHAM v6 with a horizontal resolution of 1.875° (longitude) by 1.875° (latitude), the ocean model NEMO v3.4 with a 1° by 1° horizontal resolution, the sea ice model CICE v4.1, and the coupler version 3 of the Ocean-Atmosphere–Sea–Ice–Soil Model Coupling Toolkit (OASIS3.0-MCT). In the previous model version, there were no vegetation dynamics or carbon cycle, and there was a large radiation energy imbalance. In the NESMv3, the atmospheric model was coupled with the land surface model, which contains the dynamic vegetation scheme and carbon exchange. In addition, the resolution of the atmospheric model, and ocean and sea ice model were increased with an upgraded physical parameterization associated with convective processes (Cao et al. 2018). The NESMv3 has been used to conduct sub-seasonal to decadal climate prediction, simulate the past and future projection of climate, and explore possible mechanisms and processes responsible for climate variability (Yang et al. 2020a).

To examine the respective roles of PDO and IOBM, we conducted two pacemaker experiments with four ensemble members in each experiment. First, we nudged the monthly observed SST with a 3-day nudging timescale in the Pacific Ocean (120°E-280°E, 70°S-70°N) only for 1948 to 2013 in NESMv3. Note that the initial conditions in each ensemble member are obtained from the Coupled Model Intercomparison Project Phase 6 (CMIP6) pre-industrial run (Yang et al. 2020b). The other was the same as the first one except that the monthly observed SST was nudged in the Indian Ocean (40°E-110°E, 90°S-20°N) only for 1948-2013 in NESMv3. The atmosphere and ocean in the region outside the Pacific Ocean and the Indian Ocean are freely coupled in NESMv3, respectively. Therefore, the PDO and IOBM act as a pacemaker in each experiment, which help to identify the role of PDO and the IOBM in the PDO-IOBM relationship. The observational dataset used to nudge the observed SST was obtained from the averaged of HadISST and the ERSST v4. These two datasets were linearly combined and then interpolated to fit the model grid. While the resolution between the HadISST and ERSST v4 datasets is not the same, the PDO and IOBM indices calculated in each SST dataset are almost identical (figure not shown). To obtain more accurate SST fields, we used the average of two different observation datasets. All of the other external forcings (e.g., aerosols, greenhouse gases, etc.) varied historically.

3. Results

3.1 A non-stationary relationship between PDO and IOBM

We first show the global patterns of PDO and IOBM, and their temporal variability for the period of 1900 to 2018 on a monthly timescale (Fig. 1). Figures 1a,b display the regressed SST anomalies against the monthly PDO and the IOBM indices, respectively. When the PDO phase is positive, the cold SST anomaly extends from the western North Pacific to the central North Pacific, and the warm SST anomaly along the western coast of North America wraps the cold anomaly in a horseshoe shape in the Pacific Ocean basin. When the IOBM phase is positive, basin scale warming is dominant in the entire Indian Ocean (Fig. 1b). In addition, the spatial structures of regressed SST anomalies are similar in the Pacific and Indian Ocean basins when the phases of PDO and IOBM are positive (Figs. 1a,b). The pattern correlation coefficient between the two regressed SST anomalies against the PDO and the IOBM indices is 0.75 in the globe. This result infers that the PDO index is positively correlated with the IOBM index. Figures 1c,d show the monthly variability in each index with a 11-year running mean. Both the PDO and IOBM indices fluctuate on low-frequency time scales and they are nearly in-phase relationship. The simultaneous correlation coefficient between the monthly PDO and IOBM indices for 1900–2018 is 0.36, which is statistically significant at a 95% confidence level. In addition, the correlation coefficient between the 11-year running mean time series is 0.55, which is also statistically significant at a 95% confidence level. While the correlation coefficient does not imply the causality, this result indicates that the PDO and the IOBM is simultaneously tied.

Hereafter, the analyzed period is limited to since 1948 because the reanalysis dataset is only available since 1948 and, unless stated otherwise, the results are for the boreal winter (DJF) only. Figures 2a,b are the same as in Figs. 1c,d except those during DJF for 1948–2018. While both the PDO and IOBM are dominant on the low frequency timescales, they also have the variability less than a decade (Supplementary Fig. 1). It is evident that the 31-year running correlations between the PDO and the IOBM indices fluctuate (Fig. 2c). Note that we remove the linear trend to eliminate the anthropogenic warming trend in every 31-year window and obtain the statistical significance considering the effective degrees of freedom. When we use a 41-year window length, the weakening of the PDO-IOBM relationship is also obtained (Supplementary Fig. 2).

While the PDO and IOBM indices are positively correlated significantly in most periods, there are some decades when two indices are poorly correlated with each other. This implies that the relationship between the PDO and IOBM is not stationary. In detail, the correlation is high until the early-1970s, and then it becomes weak and slowly recovers in the recent past. In particular, the correlation for 1954–1984 is the highest at 0.64, which is statistically significant above a 95% confidence level. In contrast, the correlation coefficient of 0.25 for 1976–2006 is the smallest, which is not statistically significant. While the PDO has gone through regime shifts in 1976 and 1998 (Hare and Mantua 2000; Peterson and Schwing 2003), the number of a positive and a negative phase of PDO is 19 and 12, respectively, during 1976–2006. This indicates that a single phase of PDO is not dominant in a period when the PDO-IOBM relationship is weak. To further understand the PDO-IOBM relationship, we also calculate the relationship of ENSO-IOBM. El Nino and Southern Oscillation (ENSO) is the most dominant SST variability in the

tropical Pacific on interannual timescales, and it is known that ENSO interacts with the Indian Ocean (Alexander et al. 2002; Klein et al. 1999; Lau and Nath 1996; Saji et al. 2006). Figure 2d displays the time series of NINO3.4 SST index during DJF for 1948–2018. We find that the 31-year running correlation between the NINO3.4 index and the IOBM is nearly stationary during the entire analyzed period (Fig. 2e). We infer that the non-stationary relationship between the PDO and the IOBM could be from the PDO which is not related to the ENSO.

We further analyze a long term period (1,100 years) of simulation from a Community Earth System Model (CESM) (Kay et al. 2015) under a pre-industrial atmospheric condition to avoid a sampling issue of PDO-IOBM relationship. Following the same methodology applied to the observation, we obtain the PDO and IOBM indices from a CESM and then examine their relationship. Figures 3a,b display the regressed SST anomalies against the PDO and IOBM index, respectively, in a CESM, which are similar to the observation. To verify a non-stationary relationship of PDO-IOBM with a sufficiently long window, we calculate both the 31-year and 61-year running correlation between the PDO and the IOBM (Figs. 3c,d). We find that the relationship of PDO-IOBM fluctuates on the low-frequency timescales, indicating that a non-stationary relationship of PDO-IOBM is intrinsic in a climate system in a fixed anthropogenic forcing.

In addition, we analyze the CESM large ensemble (CESM-LE) simulations for 1948–2018 (Kay et al., 2015). The CESM-LE array contains 35 members that are used in the same model and with the same external forcing (i.e., RCP8.5). Each CESM-LE member has a unique climate trajectory due to small differences in rounding - approximately 10^{-14} K - initial atmospheric conditions. Therefore, deviations in simulated PDO-IOBM relationship among ensemble members could be at least partly due to internal climate variability. We find that there is a large inter-member diversity to simulate the PDO-IOBM relationship (Fig. 4). While some models simulate a non-stationary relationship of PDO-IOBM like the observation, others simulate a stationary relationship of PDO-IOBM. This result implies that a non-stationary relationship of PDO-IOBM could be partly due to internal climate variability, which is consistent with the result from a long-term simulation of the pre-industrial run in a CESM.

3.2 Physical processes

To investigate the physical processes associated with the non-stationary relationship of PDO-IOBM, we select the period of 1976 to 2006, when the PDO-IOBM relationship is the weakest, and then we compare this with the results based on the entire period (1948–2018) to obtain a more reliable conclusion. It should be noted that all of the results obtained from the entire period are similar to those when the PDO-IOBM relationship was the highest during the period of 1954 to 1984 (figure not shown).

Figures 5a,b display the SST structure when the PDO phase was positive and negative, respectively, for the period from 1976 to 2006. Figures 5c,d are the same as in Figs. 5a,b except for the entire period. The spatial structures were similar to each other when the phase of PDO was positive in both for 1976–2006 and the entire period (Figs. 5a,c). Furthermore, basin scale warming in the Indian Ocean is also dominant for 1976–2006 and the entire period, respectively. However, the SST pattern during a negative phase of PDO for 1976–2006 (Fig. 5b) differs from that during the entire period (Fig. 5d). From 1976 to 2006, the

anomalous warm SST is limited in the southern North Pacific and a triangular structure of anomalous cool SST is not as well shaped in the Pacific Ocean basin compared to that during the entire period. In particular, the anomalous warm and cool SSTs are mixed over the Indian Ocean basin for the period from 1976 to 2006 (Fig. 5b), which is in contrast to that during the negative phase of PDO for the entire period in which the anomalous cool SST is dominant (Fig. 5d). This result indicates that a weakening of the relationship between the PDO and IOBM for the period from 1976 to 2006 is primarily due to the negative phase of the PDO. In the subsequent analysis, we primarily focus on the physical processes associated with the negative phase of PDO for the period from 1976 to 2006 (hereafter, referred to as –PDO_76 – 06, and then compare the results with those for the entire period (hereafter, referred to as –PDO_ALL).

We hypothesize that the structure of tropical convection could be associated with the weakening of the PDO-IOBM relationship. To examine this, we conduct a composite analysis of precipitation in –PDO_ALL and –PDO_76 – 06 (Figs. 6a,b). In addition, we also display the composites of divergent wind and velocity potential at 200hPa during –PDO_ALL and –PDO_76 – 06, respectively (Figs. 6c,d). The normal structure of precipitation in –PDO_ALL is characterized by a dry-wet-dry structure from the Indian Ocean to the central tropical Pacific (Fig. 6a). Reduced precipitation in the western-to-central tropical Pacific is associated with an anomalous cool SST in the same region in –PDO_ALL (see also Fig. 5d). In contrast, the enhanced precipitation amount in the far western tropical Pacific as well as the Maritime Continent is associated with an upper level divergence (Fig. 6c), which indicates the strengthening of the ascending motion in Walker Circulation. Concurrently, reduced precipitation in the Indian Ocean is associated with an upper level convergence (Figs. 6a,c), which is associated with the enhancement of the descending motion of Walker Circulation in the same region. We emphasize that there is a divergence over the far western tropical Pacific as well as the Maritime Continent along with a convergence in the Indian Ocean basin in the upper level (i.e., 200hPa) (Fig. 6c), which represents the normal structure of atmospheric circulations associated with the Walker Circulation in –PDO_ALL

In –PDO_76 – 06 (Fig. 6b), in contrast, the precipitation structure is different compared to that of –PDO_ALL. It is characterized by a wet-dry-wet-dry structure from the Indian Ocean to the eastern tropical Pacific. In particular, the precipitation amount is reduced in the far western tropical Pacific as well as the Maritime Continent and it increases over the Indian Ocean basin. In addition, it is slightly increased in the central tropical Pacific. Therefore, the structure of the precipitation amount between –PDO_ALL and –PDO_76 – 06 is nearly opposite despite the same negative phase of PDO. In –PDO_76 – 06, the upper level convergence extends over the Maritime Continent (Fig. 6d), leading to suppressed precipitation amounts in the same region (Fig. 6b). This result is concurrent with the upper level divergence over the Indian Ocean (Fig. 6d), which is indicative of a strengthening of the ascending motion of Walker Circulation over the Indian Ocean. This suggests that the Walker Circulation in –PDO_76 – 06 is shifted more to the west than the normal structure in –PDO_ALL.

We argue that these circulation changes over the Indian Ocean, which might be induced by the upper level convergence over the Maritime Continent, caused the mixed pattern of the anomalous warm and cool SSTs in –PDO_76 – 06 (see Fig. 5b). This is in contrast to the basin cooling in the Indian Ocean in

–PDO_ALL (see Fig. 5d). In –PDO_76 – 06, the upper level divergence caused an increase in precipitation as well as an anomalous cool SST via less penetration of shortwave radiation in the southern portion of the Indian Ocean in particular (Fig. 7a). Subsequently, the enhanced precipitation in the southern Indian Ocean causes the changes in the meridional circulation across the Indian Ocean basin, leading to the strengthening of downward motion in the northern Indian Ocean (Fig. 7b). These changes warm the Indian Ocean SST via more penetration of shortwave radiation (see Fig. 7a and Fig. 5b). It should be noted that, while the average downward shortwave radiation flux in the North Indian Ocean (0°N-20°N, 30°E-120°E) is 0.95 w/m^2, the average in the South Indian Ocean (20°S-0°N, 30°E-120°E) is -0.02 w/m^2 in –PDO_76 – 06. This result is consistent with the argument noted above. We infer that the structural change in tropical convection and its associated atmospheric circulation in the Indian Ocean, as well as the tropical Pacific, plays an important role in causing the weakening of PDO-IOBM relationship.

3.3 Pacemaker experiments

The results noted in the previous section suggest that the weakening of the PDO-IOBM relationship could have been associated with the changes in the tropical convection. To examine this argument, we conduct two pacemaker experiments using NESMv3 with four ensemble members as explained in Sect. 2. In one experiment, we nudge the monthly observed SST with a 3-day nudging timescale in the Pacific Ocean (120°E-280°E, 70°S-70°N) only for 1948 to 2013 in NESMv3, which is referred to as Pacific_Exp. In the other experiment, we do the same as for the Pacific_Exp except that the monthly observed SST is nudged in the Indian Ocean (40°E-110°E, 90°S-20°N) only for 1948 to 2013, which is referred to as Indian_Exp. We conduct the same analysis following the observations.

Figures 8a,b display the ensemble mean SST structure in –PDO_ALL and –PDO_76 – 06 in Pacific_Exp for 1948–2013. In the Pacific_Exp, the spatial structures of the composited SST in the Pacific Ocean are almost identical to the observations in both –PDO_ALL and –PDO_76 – 06 (Figs. 5b,d and Figs. 8a,b). The slight differences are due to the difference in horizontal resolution as well as the prescribed SST dataset. The most striking difference between –PDO_ALL and –PDO_76 – 06 in the Pacific_Exp is found in the SST structure in the Indian Ocean basin. While the composited SST in –PDO_ALL is dominant with a basin scale cooling, that in –PDO_76 – 06 is characterized by a basin scale warming except for the far eastern Indian Ocean. We emphasize that a positive relationship of PDO-IOBM in –PDO_76 – 06 is broken in the Pacific_Exp. This result indicates that the weakening of PDO-IOBM is primarily due to the difference in the SST forcing in the Pacific Ocean because the Indian Ocean SST is largely explained by the forcing of the Pacific Ocean SST in the Pacific_Exp. To further support this notion, we also calculate the 31-yr running correlation coefficient between the PDO and the IOBM indices in each four ensemble member of the Pacific_Exp (Fig. 8c). Similar to our observations (Fig. 2c), the relationship of PDO-IOBM is not stationary in all ensemble members. This result also indicates that the changes in the Pacific SST and its associated convection are responsible for the weakening of the PDO-IOBM relationship.

On the other hand, the results from the Indian_Exp are different from those from the Pacific_Exp. Figures 9a-c show the same as in Figs. 8a-c except for the Indian_Exp with four ensemble members. In

the Indian_Exp, the spatial structures of the composited ensemble mean SST in the Indian Ocean are almost identical to the observations in both −PDO_ALL and −PDO_76 − 06 (Figs. 5b,d, and Figs. 9a,b). In contrast to the Pacific_Exp, however, the composited SSTs in the Pacific Ocean in both −PDO_ALL and −PDO_76 − 06 in Indian_Exp are different than those from the observations. The Indian_Exp does not simulate the SST structure in both −PDO_ALL and −PDO_76 − 06, that is, the triangular structure of the cool SST in the Pacific Ocean basin (Figs. 5b,d, and Figs. 9a,b). This result indicates that the Pacific Ocean SST in both −PDO_ALL and −PDO_76 − 06 is not forced by the Indian Ocean SST in the observations, because the Pacific Ocean SST is largely influenced by the forcing of the Indian Ocean SST in the Indian_Exp. Furthermore, the relationship of PDO-IOBM simulated in the Indian_Exp (Fig. 9c) is also different from the observations (Fig. 2c) and the Pacific_Exp (Fig. 9c), which supports the theory that the low-frequency fluctuations of the PDO-IOBM relationship is not due to the Indian Ocean SST forcing.

4. Summary And Discussion

In this study, we examined the non-stationary relationship of PDO-IOBM. The relationship between the two variabilities fluctuates on the low-frequency time scale (i.e., one cycle in analyzed period). A long-term simulation of climate model and its large ensemble simulations indicated that the non-stationary relationship of PDO-IOBM is intrinsic in a climate system and it could be at least partly due to internal climate variability. In the observation, we found that, while the PDO and the IOBM indices were significantly, positively correlated in most periods, there were some periods when its relationship was weak (i.e., 1976–2006). By comparing the SST structures in the Pacific and Indian Ocean basins during positive and negative phases of PDO for 1976 to 2006 and for the entire period, respectively, we found that a weakening of the relationship between the PDO and IOBM for 1976 to 2006 was primarily due to the negative phase of PDO.

We further analyzed the structure of tropical convection as well as the atmospheric circulation at the upper level in −PDO_76 − 06 and −PDO_ALL. We found that there are structural differences in precipitation between −PDO_76 − 06 and −PDO_ALL, which were closely associated with those of the upper level divergence/convergence. This result emphasized the importance of the tropical convection structure in the two ocean basins. To test this argument, we analyzed two pacemaker experiments in which the monthly observed SST in the Pacific Ocean (120°E-280°E, 70°S-70°N) for 1948 to 2013 was only used in NESMv3 (i.e., Pacific_Exp), and the other was the same as Pacfic_Exp except that the monthly observed SST was only prescribed in the Indian Ocean (40°E-110°E, 90°S-20°N) for 1948–2013 (i.e., Indian_Exp). We obtained a similar result in the Pacific_Exp including a non-stationary relationship of PDO-IOBM compared with the results of the reanalysis. In contrast, the Indian_Exp failed to simulate such a low frequency fluctuation of the PDO-IOBM relationship as well as the SST structures. This result indicated that the non-stationary relationship of PDO-IOBM was primarily due to the change in the SST forcing in the Pacific.

Several recent studies indicated that Atlantic variability may change the interactions between the Indian Ocean and the Pacific (Levine et al. 2017; Li et al. 2016; McGregor et al. 2014; Zhang and Delworth 2007).

Although we did not examine the details on the role of the Atlantic Ocean in the current study, we compared the Atlantic Multi-decadal Oscillation (AMO) index with the relationship of PDO-IOBM (Fig. 10). The AMO index is defined as the SST anomalies averaged in the Atlantic Ocean basin (0°-60°N, 280°E-360°E) (Enfield et al. 2001; Zhang et al. 2018b). The correlation coefficient between the AMO and the PDO-IOBM relationship with a 31-year window is 0.19, which is not statistically significant. However, there may exist a lagged relationship between the AMO and PDO-IOBM relationship (Fig. 10b). While a minimum of the AMO index is observed in the late-1970s, that of the PDO-IOBM relationship is observed in the late 1980s. This implies that the AMO may play a role to change the PDO-IOBM relationship with a lagged time, which is necessary to examine more details.

Declarations

Acknowledgements:

The monthly mean SST was from Hadley Centre Sea Ice and Sea Surface Temperature data set, version 1 (HadISST1) (https://www.metoffice.gov.uk/hadobs/hadisst/) and the atmospheric dataset (i.e., wind, omega, radiation) was provided by NOAA Earth System Research Laboratory, Physical Sciences Division (https://www.esrl.noaa.gov/psd/data/gridded/data.ncep.reanalysis.html). In addition, the monthly precipitation dataset can be obtained from NOAA's PRECipitation REConstruction Dataset (https://www.esrl.noaa.gov/psd/data/gridded/data.prec.html).

References

1. Alexander MA, Bladé I, Newman M, Lanzante JR, Lau N-C, Scott JD (2002) The atmospheric bridge: The influence of ENSO teleconnections on air–sea interaction over the global oceans. J Clim 15:2205–2231
2. Cai W et al (2019) Pantropical climate interactions. Science 363:eaav4236
3. Cao J et al (2018) The NUIST Earth System Model (NESM) version 3: description and preliminary evaluation. Geosci Model Dev 11:2975–2993
4. Chan JC, Zhou W (2005) PDO, ENSO and the early summer monsoon rainfall over south China. *Geophysical Research Letters*, 32
5. Chen M, Xie P, Janowiak JE, Arkin PA, Smith TM (2004) J6. 1 VERIFYING THE REANALYSIS AND CLIMATE MODELS OUTPUTS USING A 56-YEAR. DATA SET OF RECONSTRUCTED GLOBAL PRECIPITATION
6. Chen W, Feng J, Wu R (2013) Roles of ENSO and PDO in the link of the East Asian winter monsoon to the following summer monsoon. J Clim 26:622–635
7. Chowdary J, Xie S-P, Tokinaga H, Okumura YM, Kubota H, Johnson N, Zheng X-T (2012) Interdecadal variations in ENSO teleconnection to the Indo–western Pacific for 1870–2007. J Clim 25:1722–1744

8. Chowdary JS, Xie S-P, Luo J-J, Hafner J, Behera S, Masumoto Y, Yamagata T (2011) Predictability of Northwest Pacific climate during summer and the role of the tropical Indian Ocean. Climate dynamics 36:607–621
9. Cole JE, Dunbar RB, McClanahan TR, Muthiga NA (2000) Tropical Pacific forcing of decadal SST variability in the western Indian Ocean over the past two centuries. Science 287:617–619
10. Crueger T, Zinke J, Pfeiffer M (2009) Patterns of Pacific decadal variability recorded by Indian Ocean corals. Int J Earth Sci 98:41–52
11. Dong L, McPhaden MJ (2017) Why has the relationship between Indian and Pacific Ocean decadal variability changed in recent decades? J Clim 30:1971–1983
12. Enfield DB, Mestas-Nuñez AM, Trimble PJ (2001) The Atlantic multidecadal oscillation and its relation to rainfall and river flows in the continental US. Geophys Res Lett 28:2077–2080
13. Guo F, Liu Q, Yang J, Fan L (2018) Three types of Indian Ocean basin modes. Climate dynamics 51:4357–4370
14. Han W et al (2014a) Intensification of decadal and multi-decadal sea level variability in the western tropical Pacific during recent decades. Climate dynamics 43:1357–1379
15. Han W, Vialard J, McPhaden MJ, Lee T, Masumoto Y, Feng M, De Ruijter WP (2014b) Indian Ocean decadal variability: A review. Bull Am Meteor Soc 95:1679–1703
16. Hare SR, Mantua NJ (2000) Empirical evidence for North Pacific regime shifts in 1977 and 1989. Progress in oceanography 47:103–145
17. Hare SR, Mantua NJ (2001) An historical narrative on the Pacific Decadal Oscillation, interdecadal climate variability and ecosystem impacts
18. Hessl AE, McKenzie D, Schellhaas R (2004) Drought and Pacific Decadal Oscillation linked to fire occurrence in the inland Pacific Northwest. Ecological applications 14:425–442
19. Huang B et al (2015) Extended Reconstructed Sea Surface Temperature Version 4 (ERSST.v4). Part I: Upgrades and Intercomparisons. J Clim 28:911–930
20. Huang G, Qu X, Hu K (2011) The impact of the tropical Indian Ocean on South Asian high in boreal summer. Adv Atmos Sci 28:421–432
21. Huang Y, Wu B, Li T, Zhou T, Liu B (2019) Interdecadal Indian Ocean Basin Mode Driven by Interdecadal Pacific Oscillation: A Season-Dependent Growth Mechanism. J Clim 32:2057–2073
22. Kalnay E et al (1996) The NCEP/NCAR 40-year reanalysis project. Bulletin of the American meteorological Society 77:437–471
23. Kay JE et al (2015) The Community Earth System Model (CESM) Large Ensemble Project: A Community Resource for Studying Climate Change in the Presence of Internal Climate Variability. Bull Am Meteor Soc 96:1333–1349
24. Klein SA, Soden BJ, Lau N-C (1999) Remote sea surface temperature variations during ENSO: Evidence for a tropical atmospheric bridge. J Clim 12:917–932

25. Krishnamurthy L, Krishnamurthy V (2014) Influence of PDO on South Asian summer monsoon and monsoon–ENSO relation. Climate dynamics 42:2397–2410
26. Krishnamurthy V, Goswami B (2000) Indian monsoon–ENSO relationship on interdecadal timescale. J Clim 13:579–595
27. Krishnan R, Sugi M (2003) Pacific decadal oscillation and variability of the Indian summer monsoon rainfall. Clim Dyn 21:233–242
28. Levine AF, McPhaden MJ, Frierson DM (2017) The impact of the AMO on multidecadal ENSO variability. Geophys Res Lett 44:3877–3886
29. Lee S-K, Park W, Baringer Mo., Gordon AL, Huber B, Liu Y (2015) Pacific origin of the abrupt increase in Indian Ocean heat content during the warming hiatus. Nat Geosci 8(6):445–449
30. Li X, Xie S-P, Gille ST, Yoo C (2016) Atlantic-induced pan-tropical climate change over the past three decades. Nature Climate Change 6:275–279
31. Liu W et al (2015) Extended Reconstructed Sea Surface Temperature Version 4 (ERSST.v4): Part II. Parametric and Structural Uncertainty Estimations. J Clim 28:931–951
32. Mantua NJ, Hare SR (2002) The Pacific Decadal Oscillation. J Oceanogr 58:35–44
33. McGregor S, Timmermann A, Stuecker MF, England MH, Merrifield M, Jin F-F, Chikamoto Y (2014) Recent Walker circulation strengthening and Pacific cooling amplified by Atlantic warming. Nature Climate Change 4:888–892
34. Newman M et al (2016) The Pacific decadal oscillation, revisited. J Clim 29:4399–4427
35. Peterson WT, Schwing FB (2003) A new climate regime in northeast Pacific ecosystems. *Geophysical research letters*, 30
36. Qu X, Huang G (2012) Impacts of tropical Indian Ocean SST on the meridional displacement of East Asian jet in boreal summer. Int J Climatol 32:2073–2080
37. Rayner N et al (2003) Global analyses of sea surface temperature, sea ice, and night marine air temperature since the late nineteenth century. *Journal of Geophysical Research: Atmospheres*, 108
38. Saji N, Xie S, Yamagata T (2006) Tropical Indian Ocean variability in the IPCC twentieth-century climate simulations. J Clim 19:4397–4417
39. Schneider N, Cornuelle BD (2005) The forcing of the Pacific decadal oscillation. J Clim 18:4355–4373
40. Schott FA, Xie SP, McCreary JP Jr (2009) Indian Ocean circulation and climate variability. *Reviews of Geophysics*, 47
41. Sui CH, Chung PH, Li T (2007) Interannual and interdecadal variability of the summertime western North Pacific subtropical high. *Geophysical research letters*, 34
42. Ummenhofer CC, D'Arrigo RD, Anchukaitis KJ, Buckley BM, Cook ER (2013) Links between Indo-Pacific climate variability and drought in the Monsoon Asia Drought Atlas. Climate dynamics 40:1319–1334

43. Waliser DE, Murtugudde R, Lucas LE (2003) Indo-Pacific Ocean response to atmospheric intraseasonal variability: 1. Austral summer and the Madden-Julian Oscillation. *Journal of Geophysical Research: Oceans*, 108
44. Wang L, Chen W, Huang R (2008) Interdecadal modulation of PDO on the impact of ENSO on the East Asian winter monsoon. *Geophysical Research Letters*, 35
45. Xie S-P, Hu K, Hafner J, Tokinaga H, Du Y, Huang G, Sampe T (2009) Indian Ocean capacitor effect on Indo–western Pacific climate during the summer following El Niño. J Clim 22:730–747
46. Yang J, Liu Q, Xie SP, Liu Z, Wu L (2007) Impact of the Indian Ocean SST basin mode on the Asian summer monsoon. *Geophysical Research Letters*, 34
47. Yang Y-M, An S-I, Wang B, Park JH (2020a) A global-scale multidecadal variability driven by Atlantic multidecadal oscillation. National Science Review 7:1190–1197
48. Yang Y-M, Wang B, Cao J, Ma L, Li J (2020b) Improved historical simulation by enhancing moist physical parameterizations in the climate system model NESM3. 0. *Climate Dynamics*1-22
49. Zhang R, Delworth TL (2007) Impact of the Atlantic multidecadal oscillation on North Pacific climate variability. *Geophysical Research Letters*, 34
50. Zhang Z, Sun X, Yang X-Q (2018a) Understanding the interdecadal variability of East Asian summer monsoon precipitation: Joint influence of three oceanic signals. *Journal of Climate*
51. Zhang Z, Sun X, Yang X-Q (2018b) Understanding the interdecadal variability of East Asian summer monsoon precipitation: Joint influence of three oceanic signals. J Clim 31:5485–5506

Figures

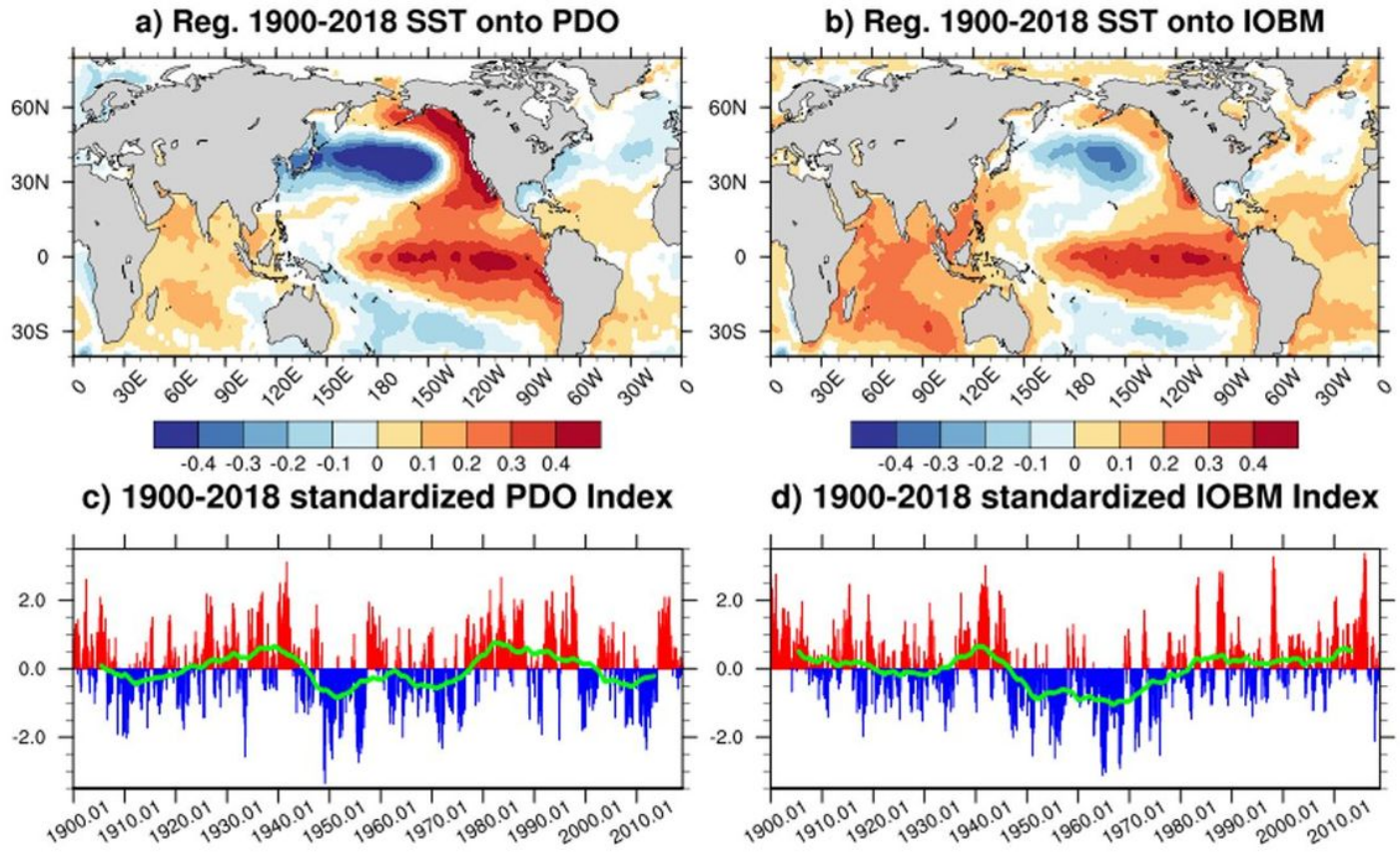

Figure 1

The spatial structures of the regressed SST anomalies against the monthly PDO index (a) and the IOBM index (b) from 1900 to 2018. (c), (d) display the time series of the monthly PDO and IOBM indices, respectively, from 1900 to 2018. The green lines in (c), (d) denote the 11-year running mean time series of each index. Shading in Fig. 1a,b represents the region where the statistical significance is at a 95% confidence level

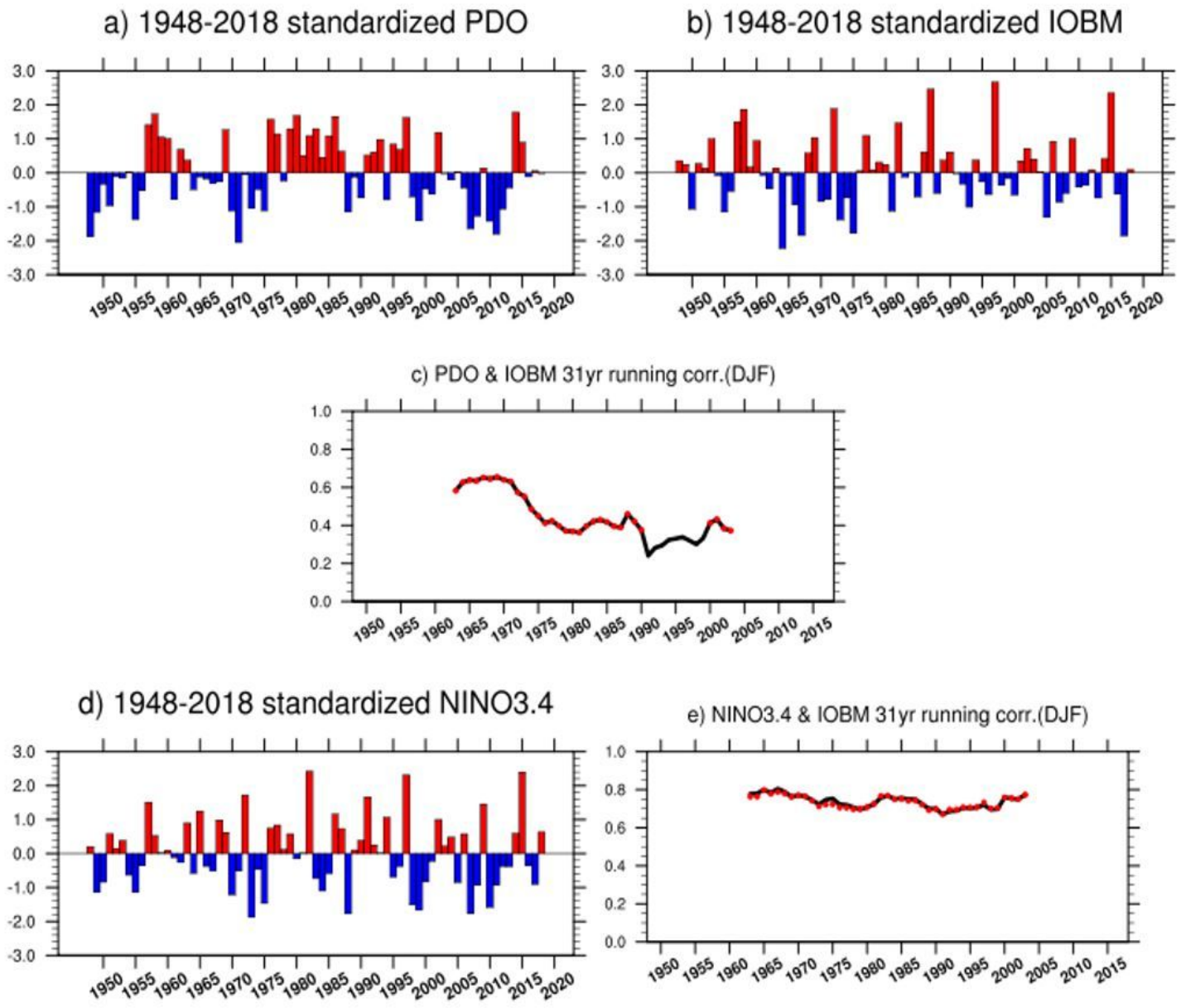

Figure 2

Time series of the (a) PDO and (b) IOBM d) NINO3.4 indices for DJF from 1948 to 2018. The 31-year running correlation using the (c) unfiltered PDO and the IOBM indices, and (e) the Nino3.4 and the IOBM indices. Red dots in Figs. 2c,e denote a statistically significant correlation coefficient at a 95% confidence level

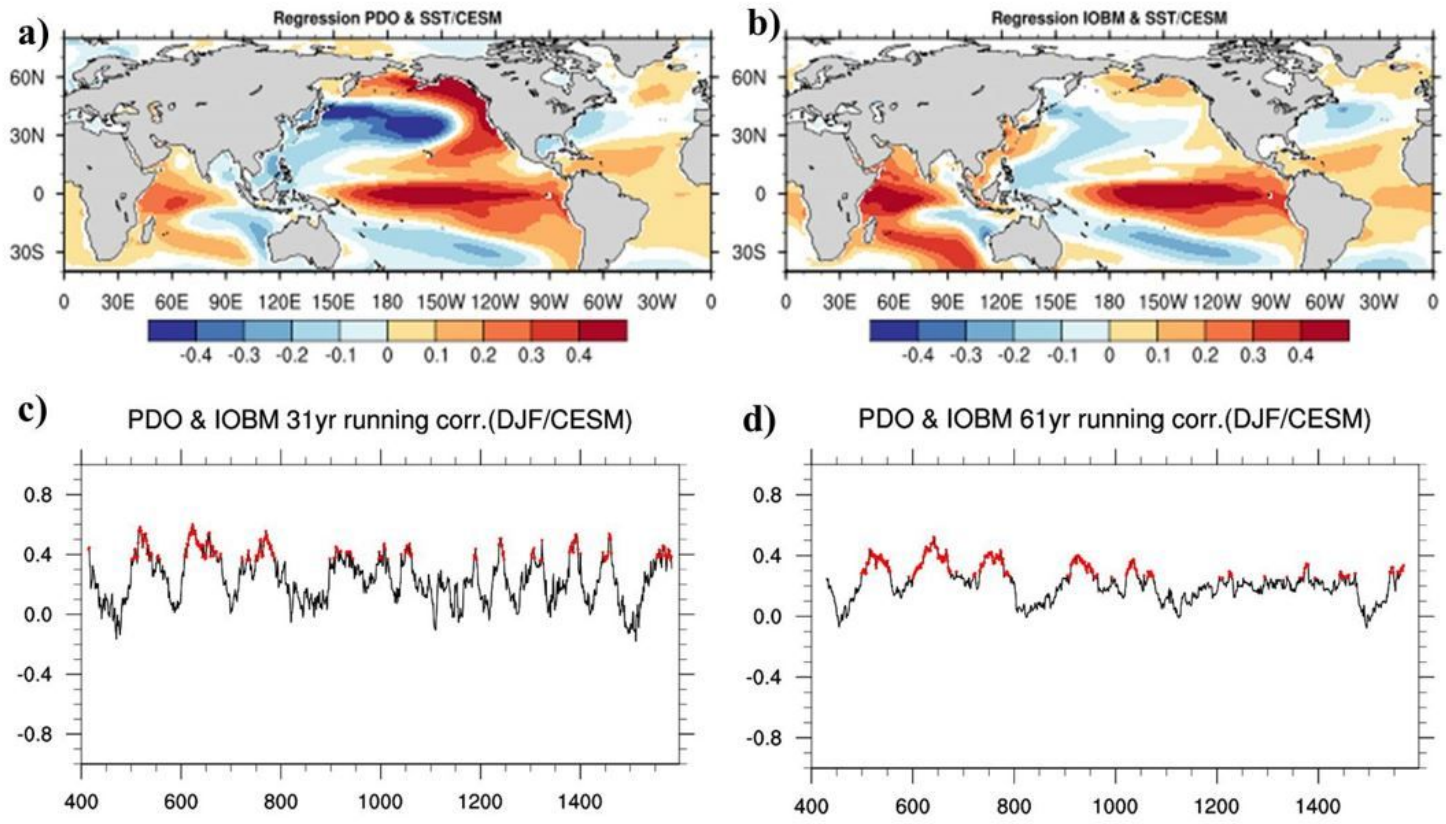

Figure 3

The SST spatial structure of the regressed SST anomalies against the (a)PDO and (b)IOBM index during DJF based on a long term period (1,100 years) of simulation in a CESM. Shading in Fig. 4a,b represents the region where the statistical significance is at a 95% confidence level. (c)The 31-year running correlations and (d) 61-year running correlations between the PDO and the IOBM without filtering. Red dots denote a statistically significant correlation coefficient at the 95% confidence level within the 31-year running window

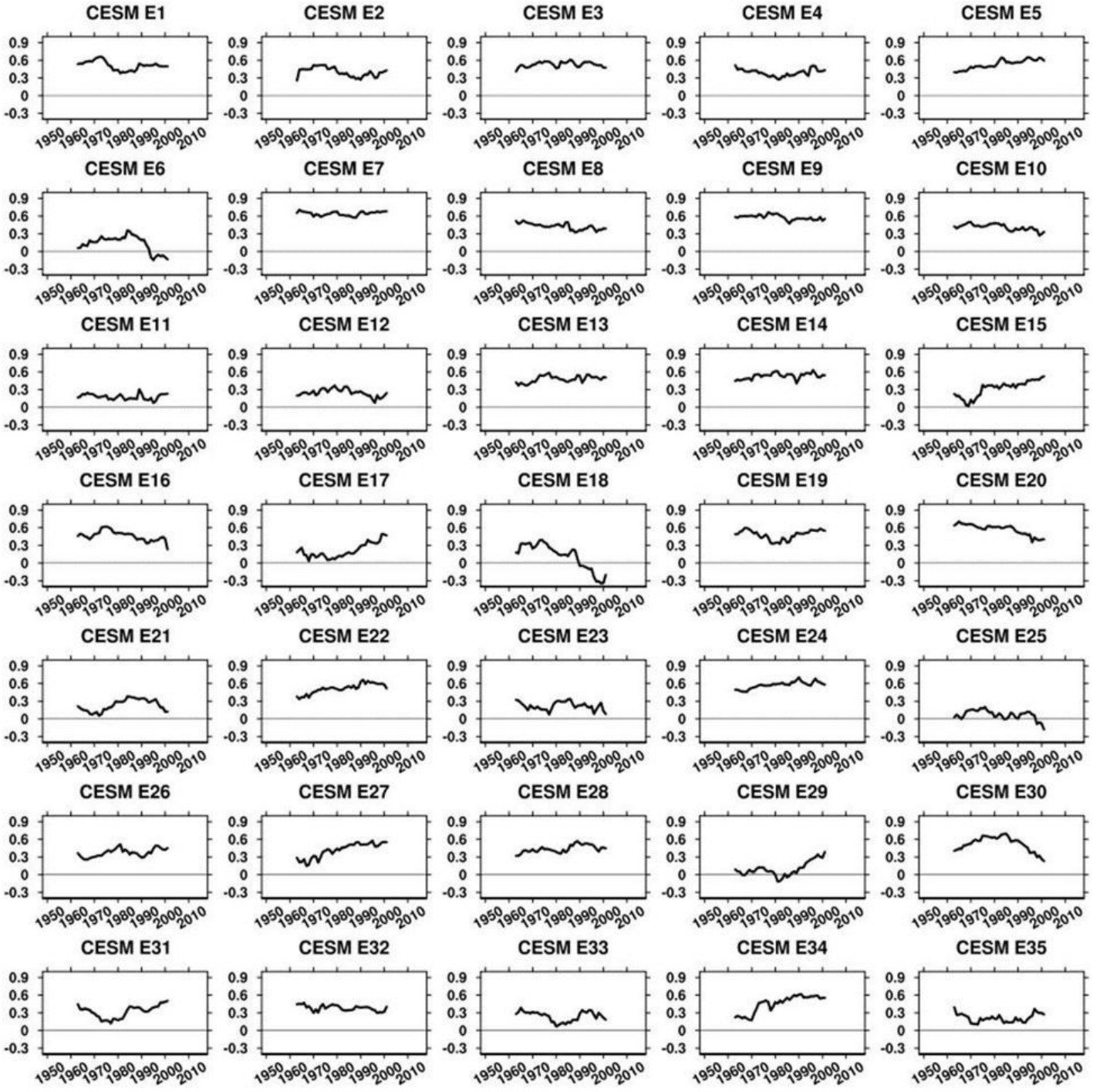

Figure 4

The 31-year running correlations between the PDO and the IOBM in each 35 CESM ensemble members during DJF for 1948-2018

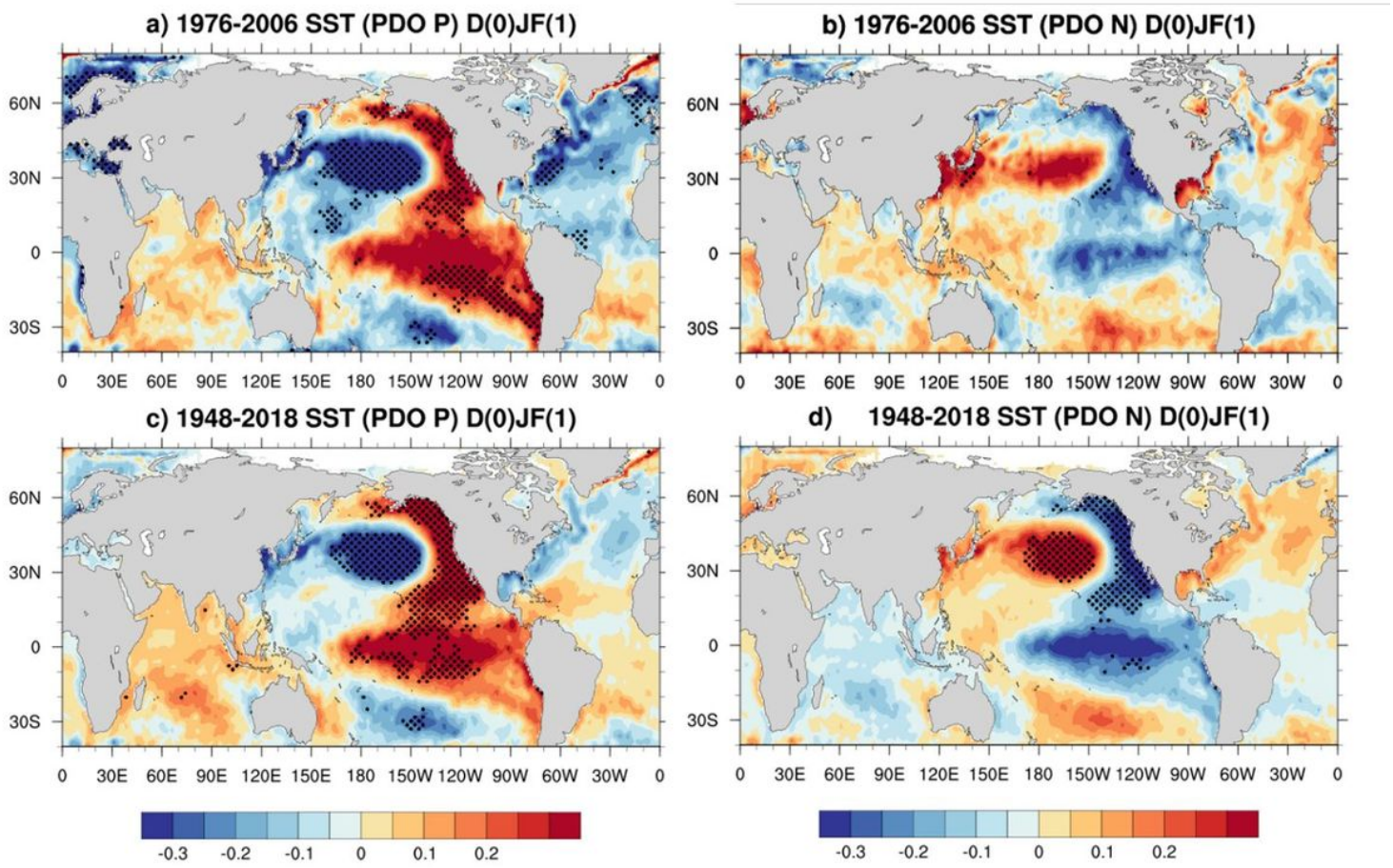

Figure 5

Composited SST maps when the PDO phase is positive (a) and negative (b) for 1976 to 2006. Figures 5c,d are the same as Figs. 6a,b, except for the entire period (1948-2018). Dots in Fig. 5 denote statistical significance at a 95% confidence level

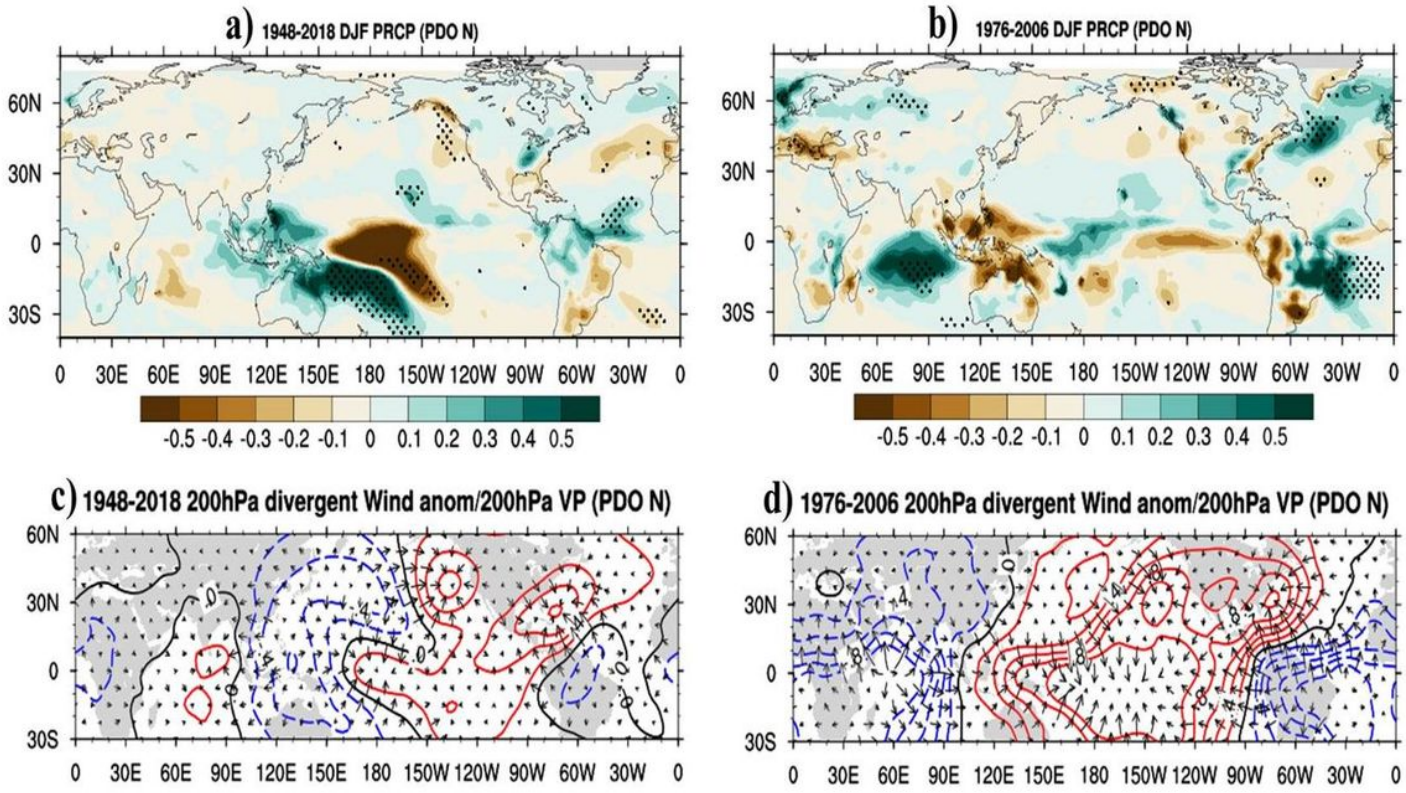

Figure 6

Composited precipitation maps in (-) PDO_ALL (a) and (-) PDO_76-06 (b). Figures 6c,d are the same as Figs. 6a,b except for the composited velocity potential and divergent wind maps in (-) PDO_ALL and (-) PDO_76-06, respectively

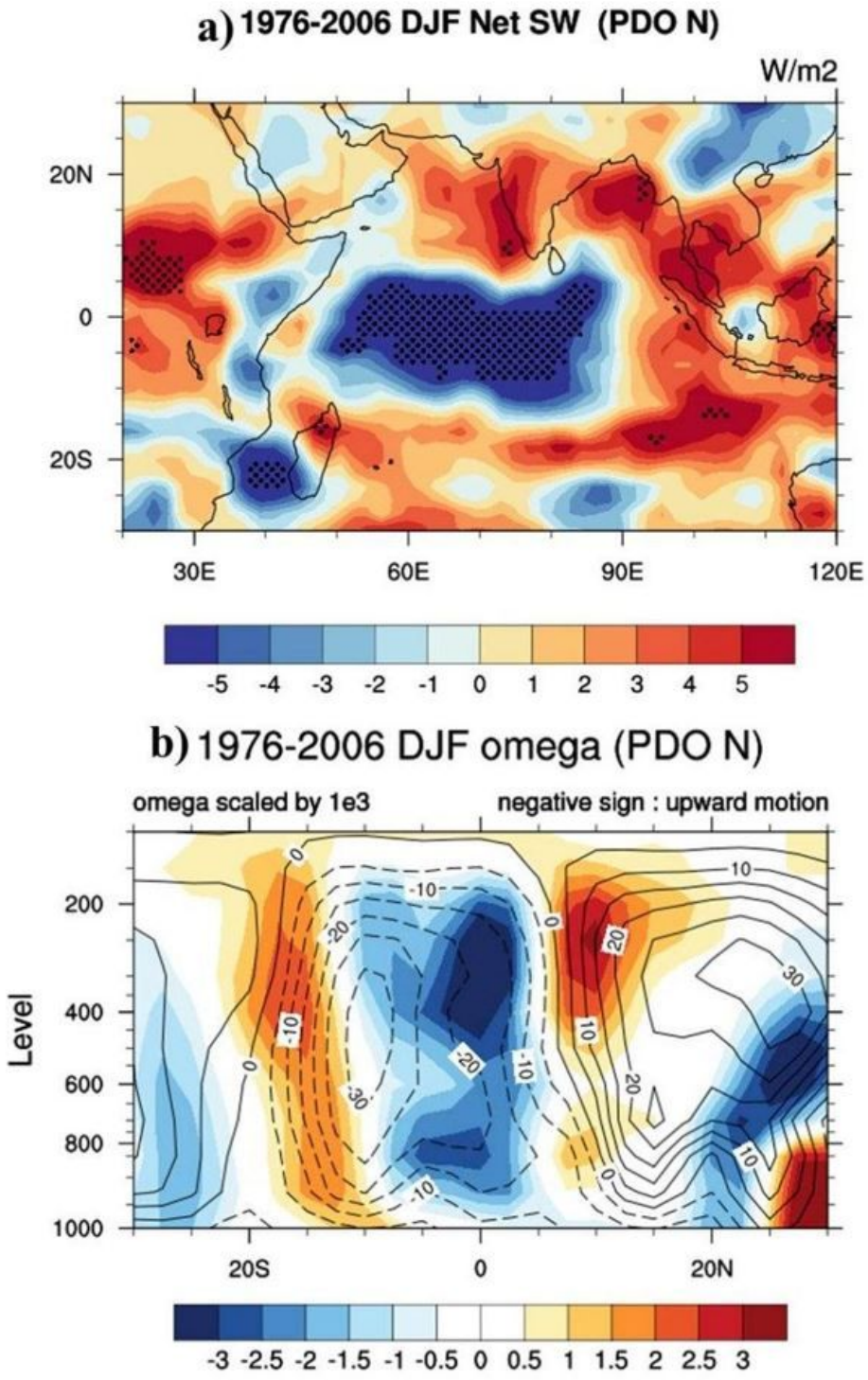

Figure 7

(a) The composited net shortwave radiation maps in (-) PDO_76-06 (a). Figure 8b is the same as Fig. 7a except for the zonally (30-E-120 E) averaged omega in (-) PDO_76-06 (shading). Dots in Fig. 7a indicate the statistical significance at a 90% confidence level. Solid (dashed) lines in Fig. 7b denote the climatological (1948-2018) descending (ascending) motion. The units are watt/m2 in Fig. 7a and Pascal/s in Fig. 7b. It should be noted that we multiplied 103 by the original value

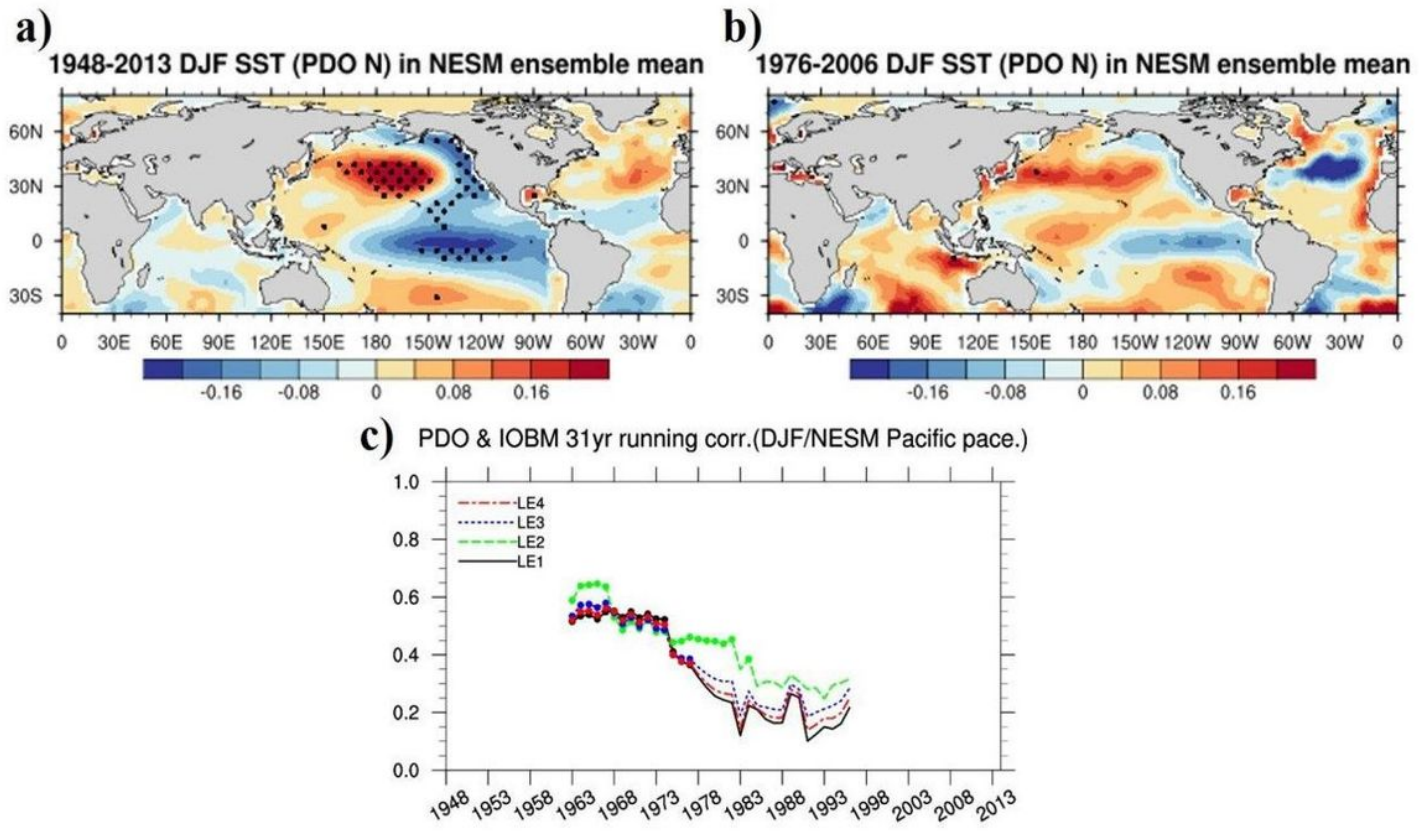

Figure 8

The ensemble mean composited SST maps (a) in (-) PDO_ALL and (b) in (-) PDO_76-06 in the Pacific_Exp. (c) The 31-yr running correlation between the PDO and the IOBM indices for DJF from 1948 to 2013 in each ensemble. The dots denote statistical significance at a 95% confidence level

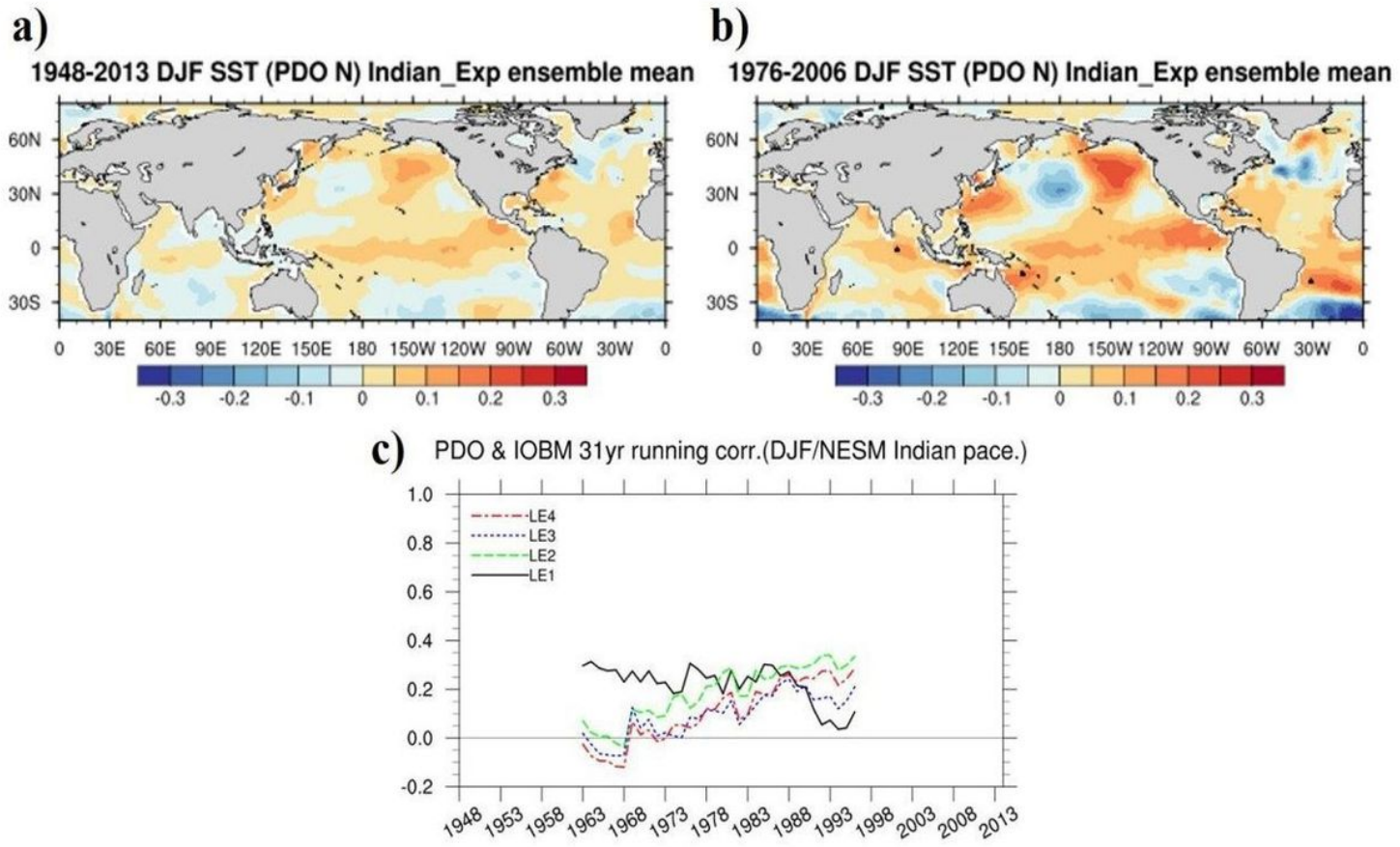

Figure 9

a-c are the same as Figs. 8a-c except for the Indian_Exp.

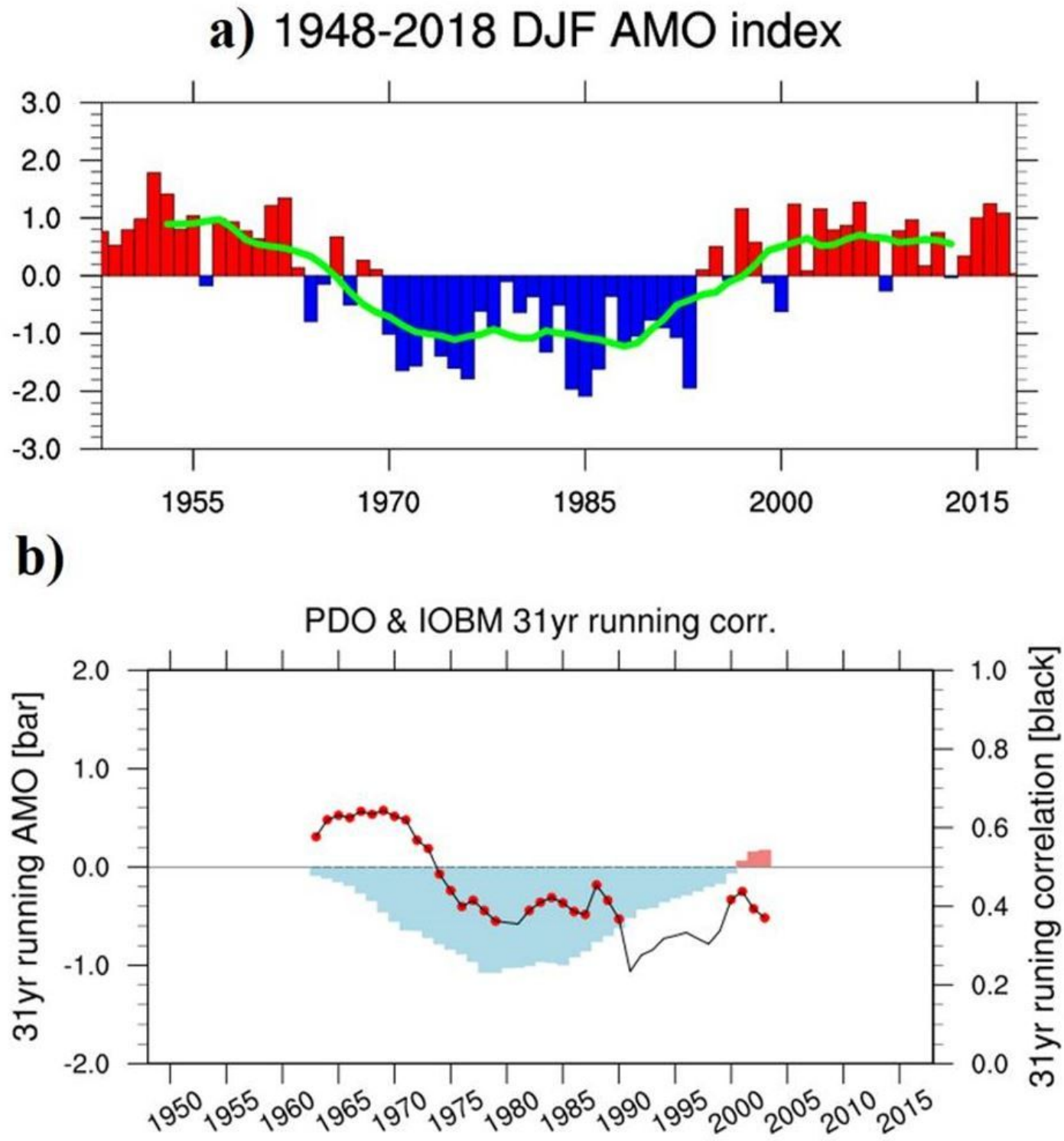

Figure 10

The normalized time series of the (a) unfiltered AMO index (bar) and 11yr running averaged AMO index (green line) for DJF from 1948 to 2018. (b) The 31yr running correlation between the PDO and the IOBM indices (black line) and the 31yr running averaged AMO index (red line)

Supplementary Files

This is a list of supplementary files associated with this preprint. Click to download.

- CDPDOIOBMSI2021.06.17.docx